HAL open science

# Correlation between Near-Field Scan Immunity and Radiated Susceptibility at Integrated Circuit Level

Alexandre Boyer, Nicolas Nolhier, Fabrice Caignet, Sonia Ben Dhia

▶ To cite this version:

Alexandre Boyer, Nicolas Nolhier, Fabrice Caignet, Sonia Ben Dhia. Correlation between Near-Field Scan Immunity and Radiated Susceptibility at Integrated Circuit Level. International Symposium on Electromagnetic Compatibility (EMC Europe 2022), Sep 2022, Goteborg, Sweden. 10.1109/EMCEurope51680.2022.9900970 . hal-03773209

HAL Id: hal-03773209
https://hal.laas.fr/hal-03773209

Submitted on 9 Sep 2022

**HAL** is a multi-disciplinary open access archive for the deposit and dissemination of scientific research documents, whether they are published or not. The documents may come from teaching and research institutions in France or abroad, or from public or private research centers.

L'archive ouverte pluridisciplinaire **HAL**, est destinée au dépôt et à la diffusion de documents scientifiques de niveau recherche, publiés ou non, émanant des établissements d'enseignement et de recherche français ou étrangers, des laboratoires publics ou privés.

# Correlation between Near-Field Scan Immunity and Radiated Susceptibility at Integrated Circuit Level

A. Boyer, N. Nolhier, F. Caignet, S. Ben Dhia
*LAAS-CNRS*
*Univ. de Toulouse, INSA, UPS, LAAS)*
Toulouse, France
alexandre.boyer@laas.fr, nolhier@laas.fr,
fcaignet@laas.fr, sonia.ben.dhia@laas.fr

***Abstract*— Near-Field Scan Immunity (NFSI) is a powerful technique to identify root-cause of failures produced during radiated immunity tests at IC level. However, a prediction method of the radiated immunity level from NFSI results is still missing. Such a method would help designers to anticipate risks of radiated immunity non-compliance after a near-field scan campaign. This paper presents the equivalence between far-field and near-field coupling on an electrically short interconnected in order to derive an estimator of IC radiated susceptibility in TEM/GTEM cell from NFSI. This estimator is tested and validated on near-field scan results on a bandgap reference. Moreover, the proposed approach relies on calibrated injection probes. As no technical specification defines a standard calibration method, this paper addresses also this issue.**

***Keywords*— *Near-field scan, radiated susceptibility, TEM/GTM cell, integrated circuit, near-field probe calibration***

## I. Introduction

Near field scan immunity (NFSI), as detailed by its IEC technical specification [1], is a powerful method to analyze susceptibility at IC level [2]. It reveals coupling areas that can lead to failures and can assist EMC expert to identify root-cause of failures that may trigger during radiated immunity (RI) tests or near-field (NF) coupling with surrounding devices. However, a question has been hardly addressed: the relationship between measurement results from NFSI and those of typical RI tests with plane wave illumination, e.g. in TEM/GTEM cells [3]. Such a relationship would not only help designer to locate sensitive pins and diagnose origin of failures with NFSI, but also estimate the RI level and anticipate risks of non-compliance. It was addressed recently in [4] to correlate RI tests in anechoic chamber and NFSI at PCB level. However, the proposed approach requires preliminary RI and NFSI tests performed on an initial PCB version. NF-to-FF transform techniques, such as plane wave spectrum decomposition [5], have been extensively used to extrapolate radiated emission of antennas or PCB from near-field scan measurement for decades. Few comparable works have been published for RI prediction purpose. A theoretical analysis of the correlation between NFSI map and RI was also proposed in [6]. However, this approach is valid only for linear devices and requires the unpractical measurement of the phase of the induced RF voltage.

A practical method to determine RI at IC level from NFSI results is still missing. The purpose of such method is not to replace usual RI measurement method, such as TEM/GTEM cells, which is a cost-effective method to qualify RI of ICs. AS NFSI is rather an investigation tool, it aims at providing an evaluation of RI of an IC at the end of a failure root-cause analysis. The purpose of this paper is to present and validate a NFSI-based estimator of IC immunity to plane-wave illumination produced in TEM/GTEM cells, which is the typical method used to assess IC susceptibility to FF radiated disturbance. This estimator should provide the worst-case RI level, in order to assess radiated susceptibility (RS) risk at the end of a NFSI campaign. Due to the small size of IC packages, package pins can be considered electrically small up to several GHz, which simplifies the comparison of FF and NF coupling expressions. The proposed approach requires a knowledge of the fields produced by the NF probe. A preliminary probe calibration is essential to determine the field produced by the NF probe at a given distance and for a given excitation. As no standard calibration method still exists for NF injection probes, this paper also addresses this issue.

This paper is organized as follows: the injection probe calibration process is described in Section II. The equivalence between FF and NF couplings for short IC interconnects is discussed in Section III and the NF-based FF-coupling estimator is derived. The estimator is tested on an experimental case study based on a bandgap reference. The experimental setup is presented in Section IV. Finally, in Section V, NFSI results are presented. RI level is estimated from the NF-based FF-coupling estimator and compared with GTEM cell results.

## II. Calibration of Near-Field Injection Probes

### A. Proposed Calibration Method

As suggested in [7] and [8], due to their small sizes, a convenient approach consists in assuming that injection probes are equivalent to elementary dipoles. Based on it, a reduced set of parameters are extracted to determine their field distribution in NF region. The general calibration test set-up is described in Fig. 1. The probe is placed precisely by a near-field scanner at a controlled position ($x_P$,$y_P$) and a scan altitude $R$ above the center of a properly calibrated receiving NF probe, characterized by two parameters: its performance factor PF, which relates the measured voltage measured and the incoming field, and its effective height $h_{eff}$, i.e. the distance between the probe tip and the actual field measurement point (center in Fig. 1). The calibration consists in verifying and extracting an elementary electric or magnetic dipole model, from the measurement of field distribution around the injection probe. The expressions of the fields produced by vertically-oriented electric and magnetic dipoles are given by (1) to (4), which can be simplified according to a $1/r^3$ law for short separation distance.

$$E_r = \frac{\eta_0\beta_0^2}{2\pi} m_E cos\theta \left(\frac{1}{\beta_0^2 r^2} - \frac{j}{\beta_0^3 r^3}\right) e^{-j\beta_0 r} \approx \frac{-jm_E}{2\pi r^3}\frac{cos\theta}{\omega\varepsilon_0} \quad (1)$$

$$E_\theta = \frac{\eta_0\beta_0^2}{4\pi} m_E sin\theta \left(\frac{j}{\beta_0 r} + \frac{1}{\beta_0^2 r^2} - \frac{j}{\beta_0^3 r^3}\right) e^{-j\beta_0 r} \approx \frac{-jm_E}{4\pi r^3}\frac{sin\theta}{\omega\varepsilon_0} \quad (2)$$

This work is supported by the Nanoscan project (CNES N° 200111/00) sponsored by Centre National d'Etudes Spatiales (CNES).

XXX-X-XXXX-XXXX-X/XX/$XX.00 ©20XX IEEE

$$H_r = \frac{j\omega\mu_0\beta_0^2}{2\pi\eta_0} m_H cos\theta \left(\frac{1}{\beta_0^2 r^2} - \frac{j}{\beta_0^3 r^3}\right) e^{-j\beta_0 r} \approx \frac{m_H cos\theta}{2\pi r^3} \quad (3)$$

$$H_\theta = \frac{j\omega\mu_0\beta_0^2}{4\pi\eta_0} m_H sin\theta \left(\frac{j}{\beta_0 r} + \frac{1}{\beta_0^2 r^2} - \frac{j}{\beta_0^3 r^3}\right) e^{-j\beta_0 r} \approx \frac{m_H sin\theta}{4\pi r^3} \quad (4)$$

The injection probe model contains two parameters to be extracted: the dipole moment ($m_E$ or $m_H$), for each frequency and for a reference excitation (e.g. 1 W), and the injection height $h_{inj}$. The validity of this model can be verified experimentally if the field produced by the injection probe decays inversely to the cube of the distance r between the actual center of the receiving probe and the dipole center. The measurement is done at several separation distance R. The evolution of the E or H field is plotted vs. r, when both probes are face to face. $h_{inj}$ is adjusted to ensure that field decays according to $1/r^3$ relationship. If such a relationship is verified for a given value of $h_{inj}$, the dipole assumption is validated and the equivalent moment is extracted.

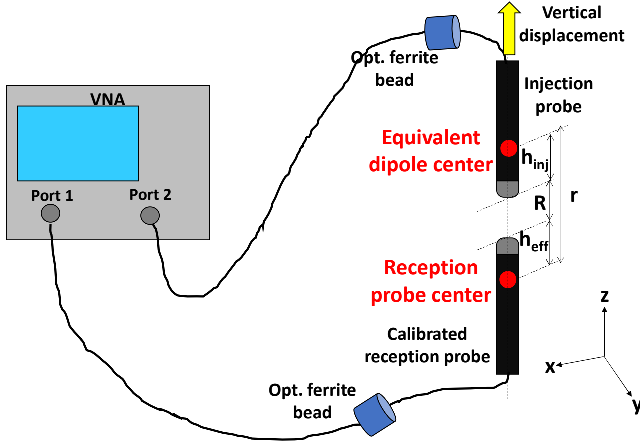


Fig. 1. Calibration set-up of injection near-field probe

The field distribution produced by the injection probe is determined from the measurement of the transmission coefficient $S_{12}$ between injection and receiving probes, e.g. using a vector network analyzer (VNA). From the measured $S_{12}$, the E or H field produced by the injection probe excited by a reference forward power $P_{forw}$ are given by (5) or (6), where $PF_E$ and $PF_H$ refer to the PF of the reception E and H-field probes.

$$E(x_0, y_0, r, \omega) = \frac{S_{12}(x_0,y_0,r\omega)}{PF_E(\omega)}\sqrt{Z_C P_{forw}} \quad (5)$$

$$H(x_0, y_0, r, \omega) = \frac{S_{12}(x_0,y_0,r\omega)}{PF_H(\omega)}\sqrt{Z_C P_{forw}} \quad (6)$$

### B. Calibration Results

The calibration procedure has been tested on two hand-made injection probes: a normal E-field probe which consists of a 4 mm long tip at the end of a semi-rigid coaxial cable, and a tangential H-field probe made of a 5 mm diameter circular loop that terminates a semi-rigid coaxial cable. The field distribution produced by these injection probes was characterized by two receiving probes: Langer EMV XFE04s E-field probe and RFR0.3-3 H-field probe. Both probes are given from 30 MHz to 3 GHz. They have been carefully calibrated up to 3 GHz according to the method described in [8]. Their $h_{eff}$ are equal to 2 and 0.9 mm respectively.

$S_{12}$ measurements have been performed between injection and receiving probes, with $R$ ranging from 0.5 to 8 mm. The evolution of the normalized $S_{12}$ according to the distance $R+h_{eff}$ is plotted in the left parts of Figs. 2 and 3. $S_{12}$ decreases with the distance, but not as rapidly as an inverse cube law. For each injection probe, $h_{inj}$ is adjusted in order to ensure that $S_{12}$ decays according to the inverse cube of $r$: $h_{inj}$ is set to 2.3 mm for the H-field probe (nearly the radius of the probe) and 3.2 mm for the E-field probe. The results are plotted on the center parts of Figs. 2 and 3, showing that the field decays with the distance in accordance with the elementary dipole model. Finally, the moments of both probes are extracted from $S_{12}$ measurement according to (52) and (55), as shown in the right parts of Figs. 2 and 3 for an excitation power of 1 W. The results show that the moment of the H-field probe is nearly constant up to 1 GHz and then tends to decrease with frequency due to the parasitic inductance of the probe. The moment of the E-field probe increases linearly with frequency at least up to 3 GHz.

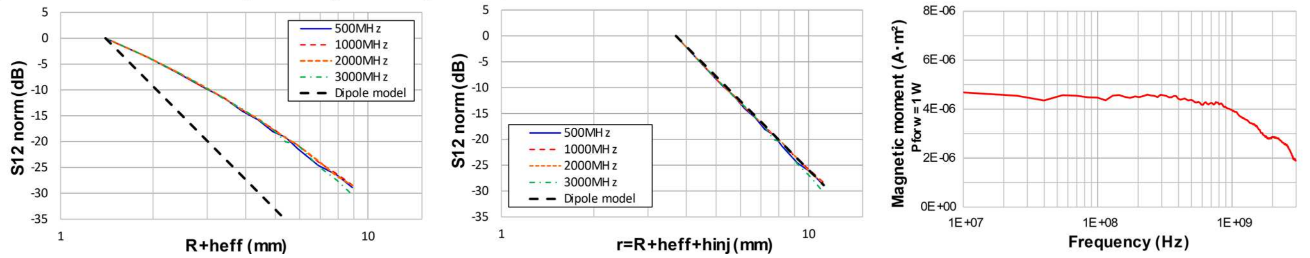


Fig. 2. Extraction of the H-field injection probe characteristics: normalized S12 vs. R+heff (left), adjustment of hinj (center), magnetic moment (right)

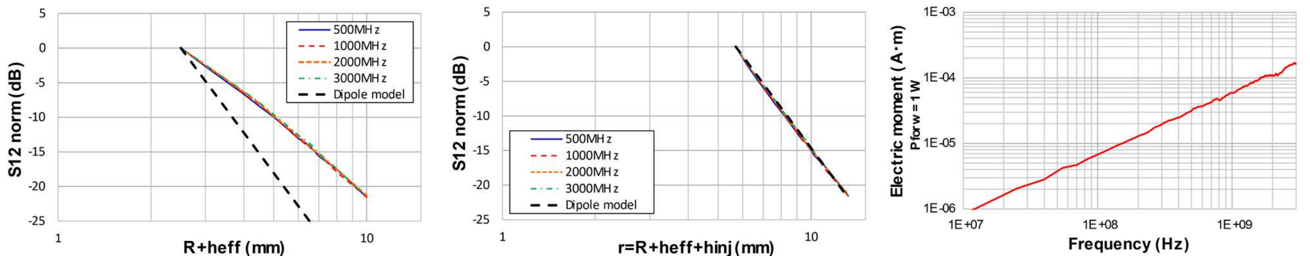


Fig. 3. Extraction of the E-field injection probe characteristics: normalized S12 vs. R+heff (left), adjustment of hinj (center), electric moment (right)

## III. Relationship between Radiated Susceptibility and Near-Field Susceptibility

Let us consider a straight and electrically-short microstrip line terminated by passive linear loads and excited by harmonic radiated disturbances (Fig. 4): either FF disturbance, i.e. plane wave illumination with random angles of incidence and polarization, or NF injection, i.e. an E or H-field probe placed in an arbitrary position above the line. The equivalence between both disturbances is analyzed by comparing the voltage induced at one terminal ports of the line ($V_{L1}$). The interconnect is supposed to be in quasi-TEM mode and the conductor and dielectric losses are neglected. Whether the incoming field is uniform or not along the line, the voltage induced on line termination can be determined according to field-to-line coupling theory, such as Taylor model [9] where the coupling of vertical E ($E_Z$) and tangential H-fields ($H_Y$) appear explicitly. In the case of a two-conductor transmission lines, the expression of the induced voltage at line end is given by (7). $\Gamma_1$ and $\Gamma_2$ are the reflection coefficients associated to termination loads, $\gamma$ the propagation constant of the line (10) and $\varepsilon_{eff}$ the effective permittivity of the line.

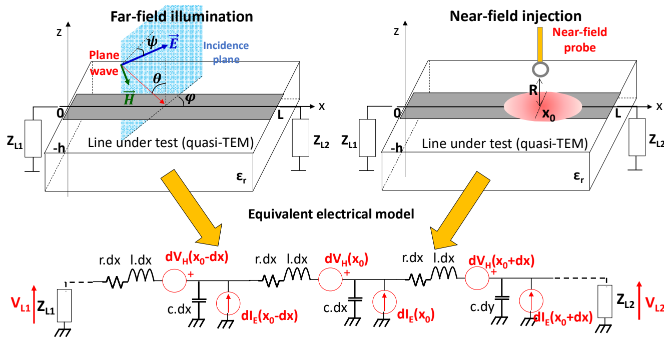


Fig. 4. Equivalent electrical model of a microstrip line exposed to a RF radiated source (plane wave or near-field source) according to Taylor model

$$V_{L1} = \int_0^L \int_{-h}^0 \frac{(1+\Gamma_1)e^{-\gamma x}}{2(1-\Gamma_1\Gamma_2 e^{-2\gamma L})}\Big(\big(1-\Gamma_2 e^{-2\gamma(L-x)}\big)dV_H(x,z) + Z_C\big(1+\Gamma_2 e^{-2\gamma(L-x)}\big)dI_E(x,z)\Big)\,dxdz \quad (7)$$

$$dV_H(x) = j\omega\mu_0 H_Y(x,z)dxdz \quad (8)$$

$$dI_E(x) = j\omega C_{line} E_Z(x,z)dxdz \quad (9)$$

$$\gamma = j\frac{\omega}{v_P} = j\frac{\omega\sqrt{\varepsilon_{eff}}}{c_0} \quad (10)$$

The induced voltage at line terminal is related to the integration of the field along the line. Although FF disturbance illuminates the line globally while NF injection is local, it is intuitive that, if NF and FF disturbance sources produce the same average field along the line, the induced voltage should be similar. From the similarities and differences between expressions of NF and FF-induced voltages, an estimator of the RI of the microstrip line from NF injection results will be derived.

### A. Far-Field Coupling on an Electrically-Short Line

Let us consider a plane wave, whose incidence direction and polarization are given by the angles θ, φ and ψ, as shown in Fig. 4. The presence of the air-dielectric interface and the ground plane leads to multiple reflections which affect the actual field that illuminates the line. When the substrate is electrically thin, the contribution of E and H-field coupling which appears in (7) can be simplified according to (11) and (12) [10] where E0 is the amplitude of the incoming E field in free space, η0 and γ0 the wave.

$$V_{LE}^{FF} = \frac{j\omega 2hE_0}{c_0\varepsilon_r}\frac{f_E\sqrt{\varepsilon_{eff}}(1+\Gamma_1)}{2(1-\Gamma_1\Gamma_2 e^{-2\gamma L})}\int_0^L e^{-\gamma_1 x}\big(1+\Gamma_2 e^{-2\gamma(L-x)}\big)dx \quad (11)$$

$$V_{LH}^{FF} = \frac{j\omega 2hE_0}{c_0} f_H \frac{(1+\Gamma_1)}{2(1-\Gamma_1\Gamma_2 e^{-2\gamma L})}\int_0^L e^{-\gamma_1 x}\big(1-\Gamma_2 e^{-2\gamma(L-x)}\big)dx \quad (12)$$

$$f_E(\theta,\psi) = sin\theta cos\psi \quad (13)$$

$$f_H(\theta,\psi) = cos\theta sin\varphi sin\psi + cos\varphi cos\psi \quad (14)$$

$$\gamma_Z = \gamma_0\sqrt{\varepsilon_r - sin^2\theta} = j\frac{\omega}{c_0}\sqrt{\varepsilon_r - sin^2\theta} \quad (15)$$

If the line is considered electrically short, (11) and (12) can be simplified into (16) and (17). The worst-case coupling arises for $\theta = \pi/2$, $\varphi = 0$ or π and $\psi = 0$ or π and when E and H-field couplings contribute in phase. The maximum amplitude of the induced voltage is given by (18). It increases linearly with frequency and proportionally to the line length.

$$V_{LE}^{FF} \approx \frac{j\omega 2hLE_0}{c_0}\frac{\sqrt{\varepsilon_{eff}}}{\varepsilon_r} f_E \frac{(1+\Gamma_1)(1+\Gamma_2)}{2(1-\Gamma_1\Gamma_2)} \quad (16)$$

$$V_{LH}^{FF} \approx \frac{j\omega 2hLE_0}{c_0} f_H \frac{(1+\Gamma_1)(1-\Gamma_2)}{2(1-\Gamma_1\Gamma_2)} \quad (17)$$

$$V_{LF\,max}^{FF} = \frac{\omega 2hLE_0}{c_0}\left|\frac{(1+\Gamma_1)}{2(1-\Gamma_1\Gamma_2)}\left(\frac{\sqrt{\varepsilon_{eff}}}{\varepsilon_r}(1+\Gamma_2)+(1-\Gamma_2)\right)\right| \quad (18)$$

### B. Near-Field Coupling on an Electrically-Short Line

Let suppose now that the disturbance is produced by a NF probe placed in close proximity (few mm) above the victim line as described in Fig. 4. Depending on the nature of the probe, they produced either a local intense E or H-field. Contrary to the FF illumination case, the field produced by the injection probe along the line is not uniform and decays rapidly with the distance. From (7), (8) and (9), the expressions of the induced voltages due to E and H-field injections are given by (19) and (20).

$$V_{LE}^{NF} = \frac{j\omega\sqrt{\varepsilon_{eff}}}{c_0}\frac{(1+\Gamma_1)}{2(1-\Gamma_1\Gamma_2 e^{-2\gamma L})}\int_0^L\int_{-h}^0 e^{-\gamma x}\Big(\big(1+\Gamma_2 e^{-2\gamma(L-x)}\big)E_Z^{NF}(x,z)\Big)\,dxdz \quad (19)$$

$$V_{LH}^{NF} = j\omega\mu_0\frac{(1+\Gamma_1)}{2(1-\Gamma_1\Gamma_2 e^{-2\gamma L})}\int_0^L\int_{-h}^0 e^{-\gamma x}\Big(\big(1-\Gamma_2 e^{-2\gamma(L-x)}\big)H_Y^{NF}(x,z)\Big)\,dxdz \quad (20)$$

In order to obtain a form similar to those in FF illumination, two simplifications are made. The first one consists in assuming that the NF coupling is extremely local, i.e. most of the coupling arises on an electrically short section centered around $x_0$. The complex exponential terms in (19) and (20) can be moved outside the integral. The second simplification consists in replacing the integral of the E or H field along z direction by the field obtained at an average height $z_0$ (comprised between -h and 0), where the field produced by the probe is equal to the average field between the line and the ground plane. With these simplifications, (19) and (20) are rewritten in (21) and (22).

$$V_{LE}^{NF} = \frac{j\omega h\sqrt{\varepsilon_{eff}}}{c_0}\frac{(1+\Gamma_1)}{2(1-\Gamma_1\Gamma_2 e^{-2\gamma L})}e^{-\gamma x_0}\big(1+\Gamma_2 e^{-2\gamma(L-x_0)}\big)\int_0^L E_Z^{NF}(x-x_0,z_0)dx \quad (21)$$

$$V_{LH}^{NF} = j\omega\mu_0 h\frac{(1+\Gamma_1)}{2(1-\Gamma_1\Gamma_2 e^{-2\gamma L})}e^{-kx_0}\big(1-\Gamma_2 e^{-2\gamma(L-x_0)}\big)\int_0^L H_Y^{NF}(x-x_0,z_0)dx \quad (22)$$

Finally, the integrals of the field along the line are replaced by the average fields giving expressions (25) and (26). If the line is considered as electrically short, they are simplified in (27) and (28). The induced voltages are proportional to the frequency and line length.

$$\overline{E_Z^{NF}(x_0)} = \frac{1}{L}\int_0^L E_Z^{NF}(x-x_0,z_0)dx \quad (23)$$

$$\overline{H_Y^{NF}(x_0)} = \frac{1}{L}\int_0^L H_Y^{NF}(x-x_0,z_0)dx \quad (24)$$

$$V_{LE}^{NF} = \frac{j\omega hL\sqrt{\varepsilon_{eff}}}{c_0}\frac{(1+\Gamma_1)e^{-\gamma x_0}}{2(1-\Gamma_1\Gamma_2e^{-2\gamma L})}\left(1+\Gamma_2e^{-2\gamma(L-x_0)}\right)\overline{E_Z^{NF}(x_0)} \quad (25)$$

$$V_{LH}^{NF} = j\omega\mu_0 hL\frac{(1+\Gamma_1)e^{-\gamma x_0}}{2(1-\Gamma_1\Gamma_2e^{-2\gamma L})}\left(1-\Gamma_2e^{-2\gamma(L-x_0)}\right)\overline{H_Y^{NF}(x_0)} \quad (26)$$

$$V_{LE\,LF}^{NF} = \frac{\omega hL\sqrt{\varepsilon_{eff}}}{c_0}\left|\frac{(1+\Gamma_1)(1+\Gamma_2)}{2(1-\Gamma_1\Gamma_2)}\right|\overline{E_Z^{NF}(x_0)} \quad (27)$$

$$V_{LH\,LF}^{NF} = \omega hL\mu_0\left|\frac{(1+\Gamma_1)(1-\Gamma_2)}{2(1-\Gamma_1\Gamma_2)}\right|\overline{H_Y^{NF}(x_0)} \quad (28)$$

### *C. Estimation of Radiated Susceptibility from Near-Field Scan Injection*

The comparison between the expressions of FF and NF-induced voltage on a microstrip line shows differences so that the exact evaluation of the FF coupling in a particular illumination condition from NFSI results is not possible rigorously. The main differences are related to the lack of the angles of arrival and polarization in the NF coupling expressions. Moreover, FF coupling is distributed while NF coupling is local, leading to different effects due to line propagation. Finally, in FF coupling, both E and H-field couplings are superimposed, contrary to NF coupling where they are separated. In practice, except if the phase is measured, it is not possible to determine how E and H-field coupling contributions measured in NFSI tests should be combined.

However, the expressions of the upper bounds of the induced voltages exhibit many similarities, especially the influence of the terminal loads and line propagation. They are sufficient to use NFSI results to upper bound the worst-case FF coupling, whatever the loading conditions, line geometry and materials. The worst-case FF and NF couplings become similar if the scaled NF-induced voltages are summed. The scaling consists in multiplying (27) by $2E_0/\left(\varepsilon_r\overline{E_Z^{NF}(x_0)}\right)$ and (28) by $2E_0/\left(\eta_0\overline{H_Y^{NF}(x_0)}\right)$ in order to determine what would be the induced voltage if the average E or H-field produced by the injection probe was identical to the plane wave excitation. The NF to FF coupling estimator is given by (29).

$$V_{L1\,LF}^{NF\to FF} = \frac{2E_0}{\overline{E_Z^{NF}(x_0)}\varepsilon_r}V_{LE\,LF}^{NF} + \frac{2E_0}{\eta_0\overline{H_Y^{NF}(x_0)}}V_{LH\,LF}^{NF} \geq V_{LF\,max}^{FF} \quad (29)$$

This estimator can also be reversed to determine the minimum amplitude of the plane wave illumination $E_{min}^{FF}$ that leads to a failure, i.e. in the worst-case coupling situation. When a failure arises, whatever the radiated disturbance nature, $V_{L1}$ is equal to $V_{Fail}$. If the failure is triggered during E and H-field injection, the terms $V_{LE\,max}^{NF}$ and $V_{LH\,max}^{NF}$ are equal to $V_{Fail}$. If the failure arises during the RS test in the worst-case coupling situation, $V_{worst}^{FF}$ is also equal to $V_{Fail}$. Injecting $V_{Fail}$ into (29) and (30) leads to (31), which gives the lower bound of $E_{min}^{FF}$ according to the average E and H field produced by the injection probes when a failure arises during NFSI.

$$V_{worst}^{FF}(E_0) \leq V_{L1}^{NF\to FF}(E_0) \quad (30)$$

$$E_{min}^{FF} \geq \frac{1}{2}\left(\frac{1}{E_{Z\,max}^{NF}\varepsilon_r\sqrt{1+\left(\frac{f}{f_C}\frac{\varepsilon_r}{\sqrt{\varepsilon_{eff}}}\right)^2}} + \frac{1}{\eta_0 H_{Y\,max}^{NF}\sqrt{1+\left(\frac{f}{f_C}\right)^2}}\right)^{-1} \quad (31)$$

## IV. Presentation of the Case Study and Experimental Setup

A micropower bandgap reference (LTC1798-2.5 from Analog Devices) is considered. It produces a 2.5 V reference voltage from a 5 V input voltage. The IC is mounted on a plastic SO8 package. The exact package encapsulation plastic material and its electrical permittivity are unknown. We assume that standard epoxy molding compound is used, with $\varepsilon_r$ ranging between 3.5 and 4. This circuit is mounted on a 10 cm ×10 cm four-layer board dedicated to TEM cell tests, with a complete ground plane on top layer. The IC is isolated on top layer, except short traces connected to the input and output pins, as shown in Fig.5. The failure criterion is a deviation of +/- 10 mV of the output voltage. Due to the small size of the package, we can assume that its package leads are electrically small up to at least 3 GHz.

RS tests are realized in a GTEM cell according to IEC62132-2, which is the most adapted and common standard method to qualify the RS of ICs [3]. The DUT can be oriented to the GTEM input connector according to four directions: 0°, 90°, 180° and 270° according to the orientation of the DUT to the cell septum. 0° and 90° directions in the GTEM cell are shown in Fig. 5. In 0° and 180° orientation, the H-field produced in the GTEM cell is oriented along y-axis, while it is oriented along x-axis in 90° and 270° orientation. NFSI tests are done with three field components: Ez, which refers to the test with normal E-field probe, and Hx and Hy with the tangential H-field probe oriented along x and y directions. Scan altitude is set at 2 mm above the PCB surface. The scan step is 2 mm along x axis and 1 mm along y axis. Tests are done from 10 MHz to 3 GHz. Two power amplifiers are used for the range 10 MHz to 1 GHz and 1 to 3 GHz, with power capability limited to 46 dBm and 44 dBm respectively. During the GTEM cell tests, the maximum E-field is limited to 1000 V/m and 800 V/m in each frequency range. The maximum power during NFSI tests is limited to 40 dBm in order to avoid overheating of the injection probes.

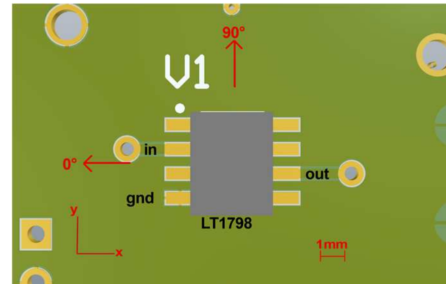


Fig. 5. Scan area and orientation of the studied bandgap reference

## V. Experimental Results

### *A. GTEM Cell Results*

Fig. 6 presents the susceptibility levels of the bandgap reference measured in GTEM cell. Results from 10 to 100 MHz are not shown as no failures were detected. Failures trigger between 200 MHz and 1.2 GHz, and around 1.7 GHz. Whatever the frequency, the disturbance induces a negative offset voltage on the bandgap reference output. Depending on the orientation of the DUT in the GTEM cell, susceptibility peaks arise either around 300 MHz or 600 MHz. The differences between the susceptibility levels measured in 0° and 90° (or 180° and 270°) orientations indicates that the H-field coupling contributes significantly. If only E-field couples, susceptibility levels will be similar whatever the DUT orientation. However, E-field coupling contributes also to the observed failures because of the differences measured between the orientations 0° and 180° (or 90° and 270°).

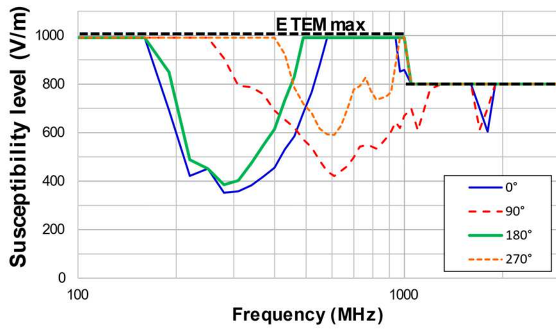


Fig. 6. Susceptibility level of the bandgap reference in GTEM cell

## *B. NFSI results*

Figs. 8 to 10 present the susceptibility maps obtained with the three injection probes. The positions of the susceptibility maxima change with the frequency. Fig. 7 shows the minimum probe excitation power required to induce a failure in the susceptibility maxima positions. Whatever the frequency, a negative offset is generated on the DUT output. During Hy injection, the coupling is mainly located on the output pin up to 350 MHz, and then extends to the input pin. Above 500 MHz, the coupling is localized between the input and the ground pins. An interesting observation is that there is nearly no offset when the probe is placed in-between these pins. The RF voltages induced on both pins tend to counterbalance. Depending on the frequency, the coupling may appear mainly on the input or the ground pin (e.g. at 1 GHz). During Hx injection, the coupling area is localized above the input and the ground pins. However, contrary to Hy injection, no offset compensation is observed. During Ez injection, the coupling area is localized above the center of the IC package whatever the frequency.

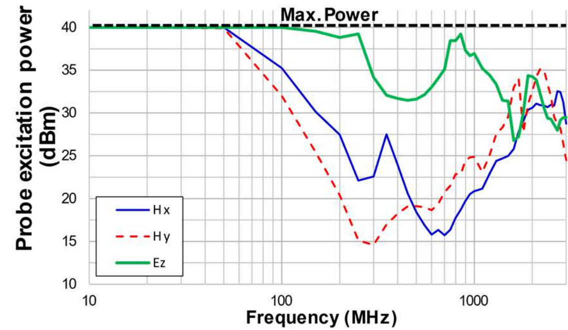


Fig. 7. Susceptibility level of the bandgap reference in NFSI tests

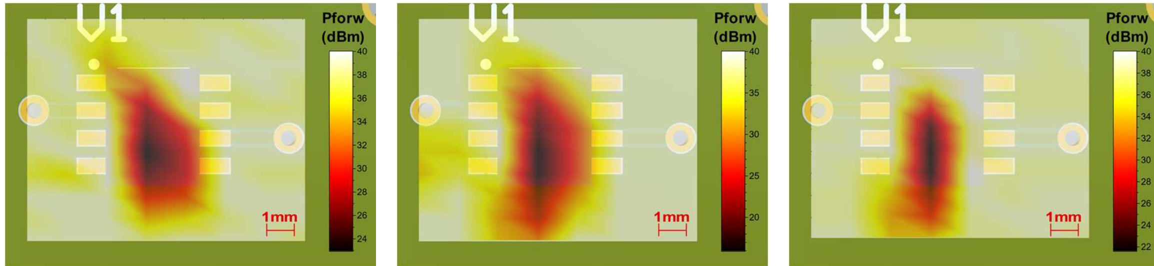


Fig. 8. Hx NFSI maps of the reference bandgap: 300 MHz (left), 600 MHz (center), 1 GHz (right)

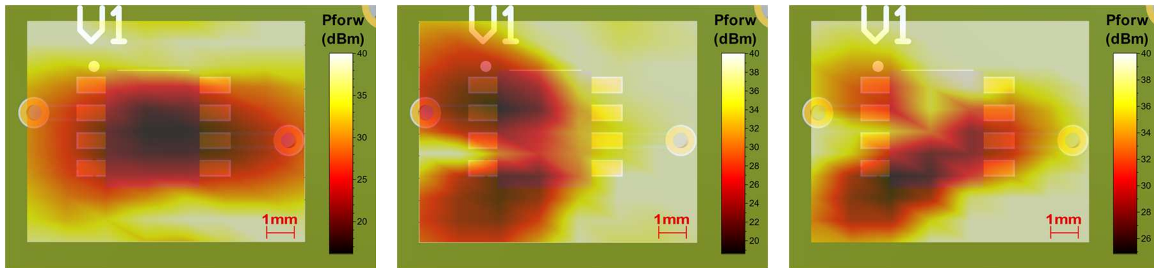


Fig. 9. Hy NFSI maps of the reference bandgap: 300 MHz (left), 600 MHz (center), 1 GHz (right)

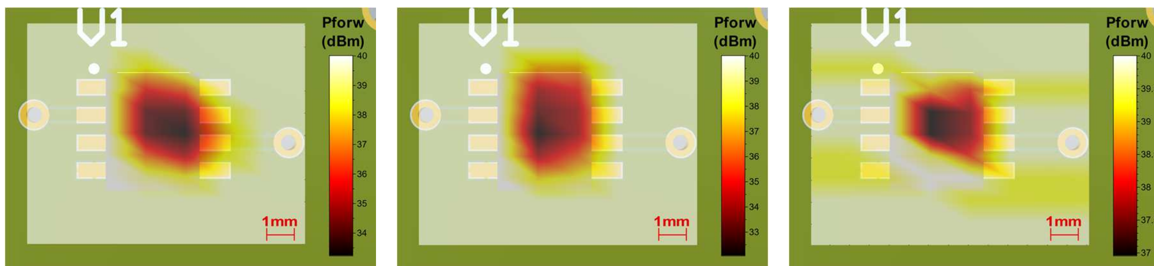


Fig. 10. Ez NFSI maps of the reference bandgap: 300 MHz (left), 600 MHz (center), 1 GHz (right)

There are some correlations between GTEM cell and NFSI results. The susceptibility peak around 300 MHz in GTEM cell tests for 0° and 180° directions is also visible in the Hy injection test. In 0° and 180° orientations, only the Hy component exists in the GTEM cell. Similarly, the susceptibility peak around 600 MHz in GTEM cell tests for 90° and 270° directions is also visible in the Hx injection test. The peak around 1.7 GHz appears both in GTEM cell and Ez injection results. However, the post-processing of NFSI results is required to clarify the link between GTEM cell and NFSI results.

### C. Radiated susceptibility estimation from NFSI results

The methodology described in Section III is used to estimate the RS level from NFSI results. It requires the identification of the minimum probe excitation power from NFSI maps, the probe calibration data, the geometrical and electrical information of the DUT. NFSI maps shows that the coupling arises on package leads. Radiated coupling on IC package pins can be modeled similarly as for a two-conductor transmission line, formed by the package lead and the ground plane below. As Taylor model is considered in this study, only the coupling on the horizontal parts of the package are considered. Package leads are assumed to be short wires at 0.8 mm above the top layer of the PCB. From NFSI maps, the sensitive pins are identified at each frequency and the coupling length is extracted. Depending if the field couples on the input and the ground pins, the coupling length $L$ is set to 4 mm for Ez, 3 or 6 mm for Hx and 4 or 8 mm for Hy. Finally, the contributions of couplings of the E and H-fields are added. However, the H-field is oriented either along x or y directions in the GTEM cell. Thus, Hx and Hy NFSI results should not be combined. RS in 0° and 180° orientations is estimated from Ez and Hy NFSI results, whereas Ez and Hx NFSI results are used to estimate RS in 90° and 270° orientations. The worst-case estimation of the RS level is made by considering the minimum value between the two previous NFSI-based estimators.

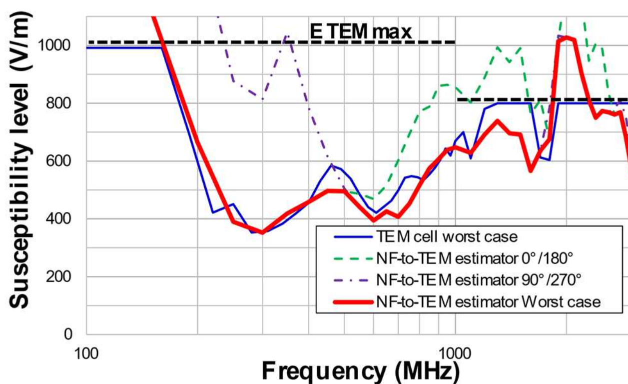


Fig. 11. Comparison between worst-case susceptibility level measured in GTEM cell and NFSI-based susceptibility estimators

This worst-case estimator is compared with the minimum RS level in GTEM cell whatever the orientation, as shown in Fig. 11. A quite good correlation is observed between 150 and 1500 MHz, where the maximum difference does not exceed 100 V/m. The susceptibility peak at 1.7 GHz is also predicted by the NFSI-based estimator with the correct order. The estimator also predicts correctly the lack of failures below 150 MHz and between 1.9 and 2.5 GHz. Differences can be explained by the uncertainty about the permittivity and the internal geometry of the IC package, but also by the differences between NFSI and TEM cell set-ups. They can also be explained by the compensation between E and H-field coupling on several pins during GTEM cell tests. However, this result shows that, even if compensation effects arise due to simultaneous coupling on several pins, it does not exist for all incoming wave orientations. Thus, the proposed NFSI-based estimator can determine the worst-case situations without an excessive overestimation.

## VI. Conclusion

NFSI is a valuable method for the analysis of root-cause of radiated susceptibility at circuit level. However, a method to extrapolate radiated immunity result from NFSI is still missing, to help user to estimate if a failure identified during a NFSI campaign can lead to a RS non-compliance problem. This paper has addressed this issue. From the equivalence between near-field and far-field couplings on a short interconnect, an estimator of the worst-case radiated immunity of an IC in TEM/GTEM from NFSI has been derived. This method requires calibration of injection probe, to determine the field they produce in close proximity. The paper has also presented a calibration method, based on the extraction of two parameters. The proposed estimation methodology has been applied successfully to predict the radiated susceptibility in GTEM cell of a reference bandgap from NFSI test results. Further works should extend the equivalence relationship between near-field and far-field coupling for electrically long interconnect, and more complex geometries in order to address the estimation of radiated immunity at PCB level.

## References

[1] IEC TS 62132-9, Integrated circuits – Measurement of electromagnetic immunity – Part 9: Measurement of radiated immunity – Surface scan method, International Electrotechnical Commission, 2014.

[2] A. Boyer, E. Sicard, S. Bendhia, “Characterization of the Electromagnetic Susceptibility of Integrated Circuits using a Near Field Scan”, Elec. Letters, vol. 43, no 1, pp. 15-16, 4th Jan. 2007, 10.1049/el:20073130

[3] IEC 61967-2 – edition 1.0: Integrated circuits - Measurement of electromagnetic emissions, 150 kHz to 1 GHz - Part 2: Measurement of radiated emissions - TEM cell and wideband TEM cell method, 2005-09-29.

[4] A. Durier, S. Ben Dhia, T. Dubois, “Comparison of Voltages Induced in an Electronic Equipment during Far Field and Near Field Normative Radiated Immunity Tests”, in Proc. of 2019 Int. Symp. On EMC - EMC Europe 2019, Barcelona, Spain, Sep. 2019.

[5] J. J. Wang, “An Examination of the Theory and Practices of Planar Near-Field Measurement”, IEEE. Trans on Antennas and Propagation, vol. 36, no. 6, June 1988, pp. 746-753.

[6] A. Boyer, “A Rigorous Method to extrapolate Radiated Susceptibility from Near-Field Scan Immunity”, in Proc. 2019 Int. Symp. on EMC - EMC Europe 2019, Barcelona, Spain, Sep. 2019.

[7] A. Boyer, "Méthode de prédiction de la compatibilité électromagnétique des systèmes en boîtier", Ph.D. dissertation, INSA Toulouse, Univ. of Toulouse, Toulouse, France, 2007.

[8] A. Boyer, N. Nolhier, F. Caignet, S. Ben Dhia, “Closed-Form Expressions of Electric and Magnetic Near-Fields for the Calibration of Near-Field Probes”, *IEEE Trans. on Instr. and Meas.*, early access, Nov. 9th 2021, pp. 1-14, 10.1109/TIM.2021.3126376

[9] C. D. Taylor, R. S. Satterwhite, W. J. Harrison, "The response of terminated two-wire transmission line excited by a non uniform electromagnetic field", IEEE Trans. on Antennas and Propagation, vol. AP-13, pp. 987-989, 1965.

[10] F. M. Tesche, M. Ianoz, T. Karlsson, EMC Analysis Methods and Computational Models, Wiley, 1996, 978-0-471-15573-7.